

## REVIEW ARTICLE

# Progress of niobate laser materials

Shoujun Ding<sup>a,b,c</sup>, Qingli Zhang<sup>a,\*</sup>, Renqin Dou<sup>a</sup>, Wenpeng Liu<sup>a</sup>, Yufei Ma<sup>d</sup>, Xiaofei Wang<sup>a</sup>, Guihua Sun<sup>a</sup>, Changjiang Gu<sup>a</sup>, Jianqiao Luo<sup>a</sup>, Renpeng Yan<sup>d</sup>, Dunlu Sun<sup>a</sup>,

**Authors' affiliations:**

- <sup>a</sup> Anhui Institute of Optics and Fine Mechanics, Chinese Academy of Sciences, Hefei 230031, PR China
- <sup>b</sup> University of Science and Technology of China, Hefei 230026, PR China
- <sup>c</sup> Chemistry and Biochemistry, Utah State University, Logan 84322, USA
- <sup>d</sup> National Key Laboratory of Science and Technology on Tunable Laser, Harbin Institute of Technology, Harbin 150001, PR China

\* Corresponding author e-mail: [zql@aiofm.ac.cn](mailto:zql@aiofm.ac.cn)

**Abstract:**

Sapphire, garnet, vanadate and tantalate crystal are the most prominent optical materials and play extremely important roles in optics, especially in lasers. Nb element belongs to the same sub-group with V and Ta elements and niobates ( $\text{LnNbO}_4$ ,  $\text{Ln}=\text{Y, Gd and La}$ ) with monoclinic structure have been proved as outstanding self-activated phosphor as early as 1960s. Due to their excellent luminescent properties, their investigations have never been interrupted. In the recent years, we focused on the single crystal growth technology of rare-earth doped niobates and a series of rare-earth doped niobate single crystals have been grown successfully using Czochralski method. Meanwhile, their structure, mechanical, luminescent properties and so on have been characterized. Continuous-wave lasers of 0.9  $\mu\text{m}$ , 1.03  $\mu\text{m}$  and 1.06  $\mu\text{m}$ , and passively Q-switched lasers using  $\text{Cr}^{4+}:\text{YAG}$  as saturable absorber have been generated successfully in Nd- and Yb-doped niobate crystals for the first time, to the best of our knowledge. In this paper, the preparation, characterization and laser performance of niobate crystals at the lasing wavelength of 1  $\mu\text{m}$ , including  $\text{YNbO}_4$ ,  $\text{GdNbO}_4$ ,  $\text{Gd}_{1-x}\text{Y}_x\text{NbO}_4$  and  $\text{Gd}_{1-x}\text{La}_x\text{NbO}_4$  single crystals doped with  $\text{Nd}^{3+}$  and  $\text{Yb}^{3+}$  are systematically reviewed by highlighting the most recent research progress.

**Keywords:** Niobate crystals; Monoclinic structure; Czochralski method; Laser performance

## 1. Introduction

Since the first stimulated optical radiation in ruby crystal laser was devised by Maiman in 1960[1], lasers have undergone a rapid development for over half a century. In 1964, especially, continuous wave (CW) laser oscillation was successfully generated using

an Nd:YAG crystal[2], and after that CW laser technology and laser gain materials has attracted tremendous attentions, which affects the application and development of lasers. In addition to CW lasers, Q-switching and mode-locking regimes are also developed rapidly for the generation of short pulse and ultrashort pulse lasers[3-6].  $\text{Nd}^{3+}$ ,

as we all know, has a typical four energy level structure and Nd-doped laser materials usually with high laser efficiency[7, 8]. Nowadays, diode-pumped solid state lasers (DPSSLs) based on Nd-doped materials have been widely applied in many fields, such as environmental detection[9], industrial processing[10], optical communication[11], medical treatment[12], and even have potential application in future nuclear-fusion[13, 14], and so on, due to their high stability, high efficiency and low maintenance[15, 16]. Among all of the traditional Nd-doped laser crystals, Nd-doped vanadate crystals and Nd:YAG are extensively investigated and widely used[17-21]. However, for vanadate crystals, it is hard to grow large-size and high-quality single crystals due to the component volatility during their Cz growth process[22]. In particular, the relatively poor mechanical and thermal properties of vanadate crystals constrain their applications in high-power laser systems[23]. For Nd:YAG crystal, it is very sensitive to the pumping wavelength due to the narrow absorption bandwidth at around 808 nm[24]. For these reasons, much effort has been paid to explore new laser crystals with good overall performance[25-28].

In recent years, much affection have been focused on the low symmetric laser crystals due to their many advantageous, such as supplying a relatively strong crystal field for active ions, improving the photoluminescence efficiency, and realizing polarized laser output[29, 30], et al. RENbO<sub>4</sub> (RE=Y, Gd, La and Lu) has been reported as a kind of low symmetric and high efficient promising luminescence material for several decades[31], which has been proved with multifunctional applications in several fields, such as phosphors[32], laser matrix[33], sensors[34], and ionic-electronic conducting materials[35], et al. In rare earth ions doped RENbO<sub>4</sub>, there exist some extent of coupling between activators and NbO<sub>4</sub><sup>3-</sup> groups, which can efficiently improve the absorption and luminescence properties and thus at-

tracted more and more groups focus on them[36]. Generally, RENbO<sub>4</sub> are crystallized with two types of phase[37]: high temperature tetragonal phase (T-type, scheelite structure with space group of I4/a) and low temperature monoclinic phase (M-type, fergusonite structure with space group of I2/a). It should be pointed out that there can undergo a reversible phase transition between monoclinic and tetragonal phase by changing the temperature[38].

Nowadays, after huge amount of tries, bulk Nd-doped and Yb-doped YNbO<sub>4</sub> (YNO) and GdNbO<sub>4</sub> (GNO) single crystals were grown successfully using the well-known Czochralski (Cz) method[7, 33, 39]. Besides, their structure and spectral properties were systemically investigated[40, 41]. Importantly, 1.06 μm CW lasers have been achieved using Nd-doped YNO and GNO single crystals and 1.03 μm CW laser has been achieved in Yb-doped GNO crystal. Using a Nd:GNO crystal, 926 nm CW laser operation based on the <sup>4</sup>F<sub>3/2</sub>→<sup>4</sup>I<sub>9/2</sub> transition of Nd ions was also generated successfully[42]. In order to broad the spectral width and improve the laser efficiency, Nd-doped Gd<sub>1-x</sub>La<sub>x</sub>NbO<sub>4</sub> (GLNO) and Gd<sub>1-x</sub>Y<sub>x</sub>NbO<sub>4</sub> (GYNO) mixed niobate laser crystals were designed and investigated with the same methods[43-45]. Furthermore, 1.06 μm passively Q-switched laser performances were generated successfully with Nd-doped GNO, GYNO and GLNO crystals. In this paper, we reviewed the growths, structures, mechanics, optical and laser properties of these novel niobate laser materials. Moreover, the electronic and optical properties of RENbO<sub>4</sub> obtained with the well-known density functional theory (DFT) calculation were also presented.

## 2. Crystal growth and characterizations

### 2.1. Single crystal growths and structures

In this work, all the niobate laser crystals were grown by Cz method using an

up-weighting JGD-60 furnace equipped with an automatic diameter controlled system. Ultra-high purity (> 4N) raw materials were pre-dried, weighted stoichiometrically and followed with thoroughly mixing. Then, the mixtures were pressed into disks and put into an iridium crucible. To prevent the iridium from oxidation, all the crystals were grown in a nitrogen atmosphere. The rotation speed and pulling rate were 3-8 rpm and 0.3-1 mm/h, respectively, for all the growth processes. The as-grown Nd-doped YNO, GNO, GYNO and GLNO are shown in Fig.1 (a). The X-ray diffraction (XRD) patterns of

the as-grown niobate crystals are shown in Fig.1 (b). As can be seen, all the diffraction peaks for them in the measured range can be well indexed with those of pure YNO (ICSD#20335) and GNO (ICSD#20408) from database, indicating that all the as-grown crystals belong to M-type structure with space group of  $I2/a$ . In M-type structure (as-shown in Fig.1 (c)), each Nb atom coordinates with four oxygen atoms forming a tetrahedron, while each rare-earth atom combines with eight oxygen atoms forming a dodecahedron.

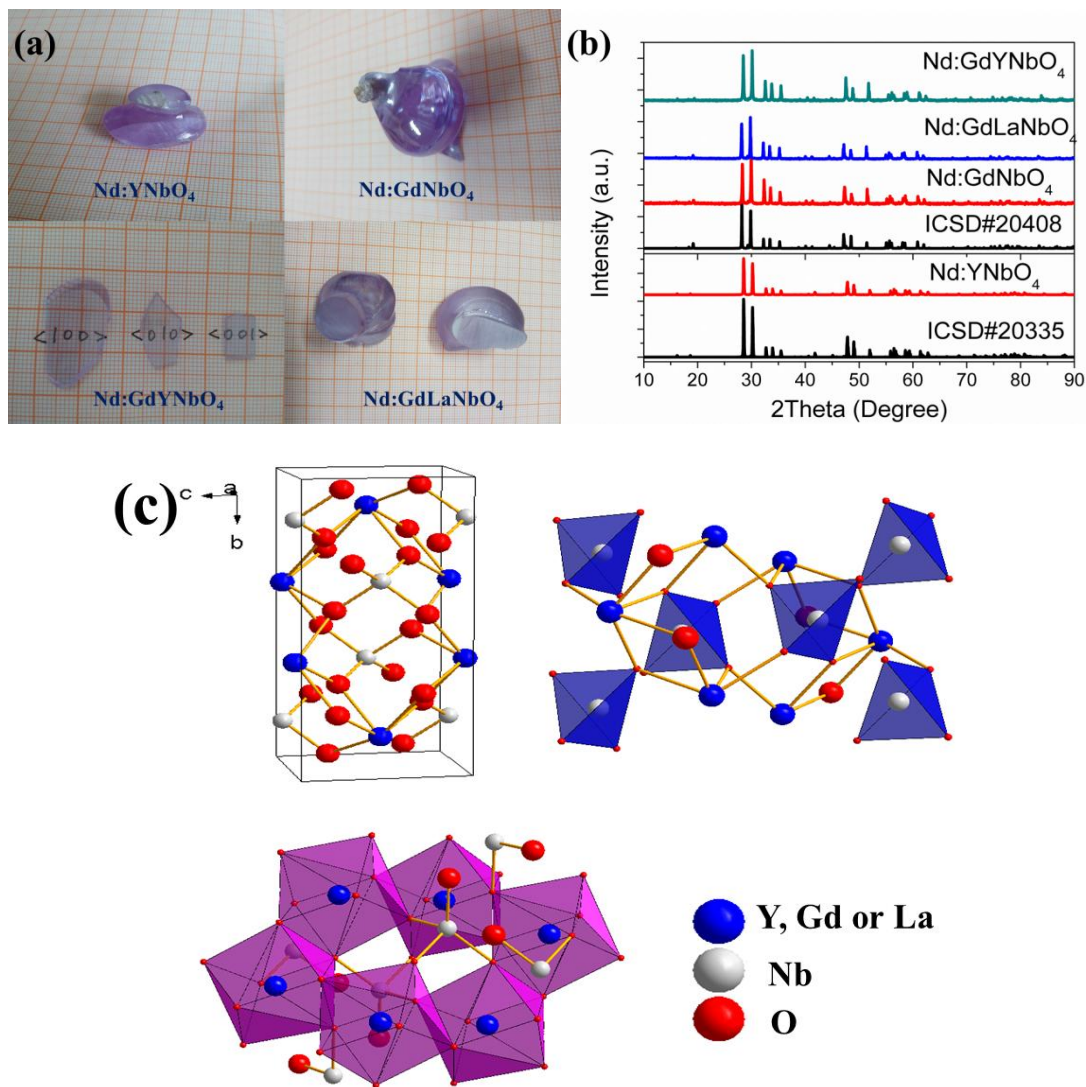


**Figure 1.** (a) Photographs of the as-grown niobate crystals; (b) X-ray diffraction peaks for Nd-doped niobate crystals and standard ICSD data from database. (c) Crystal structure and atoms coordination of M-type niobates.

## 2.2. Mechanical characterizations

It is well known that the mechanical properties for the laser crystals play a quite important role in their fabrications, coatings as well as applications[46]. Fig.2 shows the Vickers microhardness of the niobate crystals, which were obtained using a HV-1000A (HUAYIN Co., Ltd.) microhardness tester equipped with a diamond square indenter and each measurement was repeat for five

times and an average was taken. It is obviously that the Vickers hardness values for niobate crystals are all located at 800 to 1000  $\text{kg/mm}^2$  and the values are all increased with the increasing of the applied load. It is worthy to mention that Nd:GNO crystal exhibits higher hardness value than that of Nd:GLNO and Nd:GYNO, which could be attributed to the large lattice distortion in the mixed crystals.

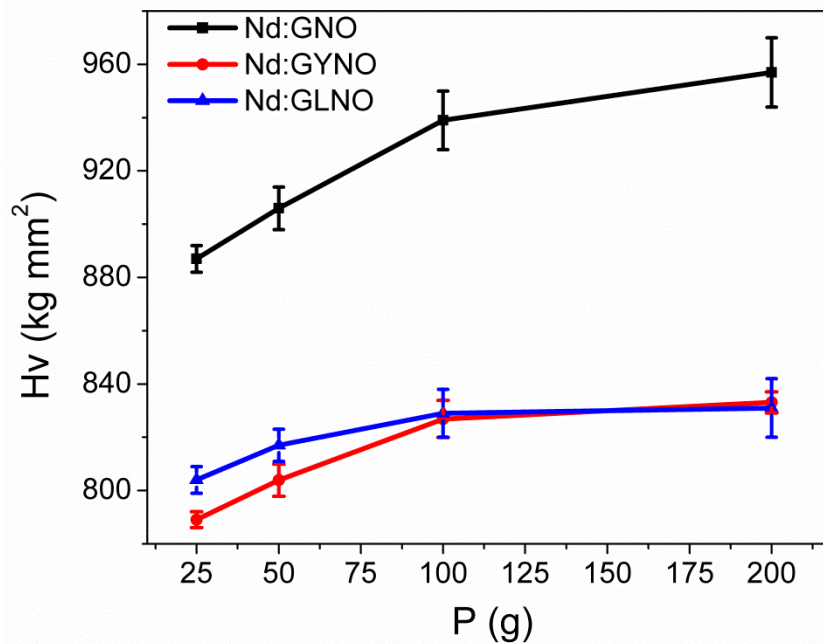


**Figure 2.** The Vickers hardness  $H_v$  versus the indentation load  $P$  for Nd-doped niobate crystals.

## 2.3. Spectral characterization

In this part, we will briefly describe the spectral properties for Nd-doped and Yb-doped niobate crystals including absorption spectra, emission spectra and fluorescence decay times.

### 2.3.1. Absorption spectra for Nd-doped crystals

Considering the as-grown niobate crystals all belongs to the monoclinic system, their absorption properties show anisotropic. Here, we just present the absorption spectra for all of them with  $b$ -orientation cut sam-

ples as shown in Fig.3, which were recorded using a PerkinElmer Lambda-950 UV/VIS/NIR spectrophotometer with a spectral interval of 0.2 nm. The eight absorption bands appeared in the spectra can be assigned to the transitions of  $\text{Nd}^{3+}$  from the ground state ( $^4\text{I}_{9/2}$ ) to excited states ( $^4\text{D}_{1/2} + ^4\text{D}_{3/2} + ^4\text{D}_{5/2} + ^2\text{L}_{15/2}$ ,  $^2\text{P}_{1/2}$ ,  $^4\text{G}_{7/2} + ^4\text{G}_{9/2} + ^2\text{K}_{13/2}$ ,  $^4\text{G}_{5/2}$ ,  $^4\text{F}_{9/2}$ ,  $^4\text{S}_{3/2} + ^4\text{F}_{7/2}$ ,  $^4\text{F}_{3/2} + ^2\text{H}_{9/2}$  and  $^4\text{F}_{3/2}$ , respectively) as denoted in the picture. It should be noted that all of these crystals are exhibits very strong absorption at around 808 nm and the full width at half maximum (FWHM) for them are all much larger than that of Nd:YAG crystal (about 2 nm)[24]. Furthermore,

Nd:GYNO and Nd:GLNO possess a slightly larger FWHM than that of Nd:YNO and Nd:GNO, which could be attribute to the inhomogeneous broadening in the mixed crystal[47, 48]. Considering the diode laser bandwidth (about 3 nm), Nd-doped niobate laser crystals can be better matched with the diode laser than Nd:YAG, which decreases the temperature dependence on the diode laser temperature control and is advantageous for improving laser efficiency. The absorption cross section  $\sigma_{ab}$  can be calculated using the formula  $\sigma_{ab}=\alpha(\lambda)/N$ , where

$\alpha(\lambda)$  denotes the absorption coefficient and  $N$  denotes the  $\text{Nd}^{3+}$  ions concentration in the crystals, which have been determined by the X-ray fluorescence spectrometer (XRF) analysis. The calculated  $\sigma_{ab}$  for these crystals is shown in the ordinate of Fig.3. The  $\sigma_{ab}$  values are  $5.7, 9.3, 11.6$  and  $10.5 \times 10^{-20} \text{ cm}^2$  for Nd-doped YNO, GNO, GYNO and GLNO at 808 nm, respectively. The largest absorption cross section for Nd:GYNO among these crystals indicating the best absorption for the pumping energy.

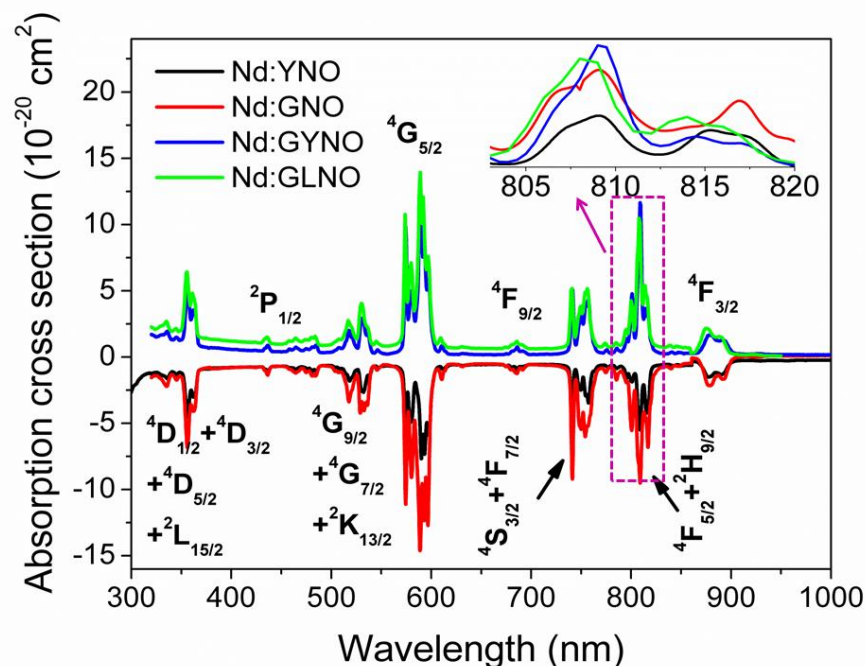


**Figure 3.** Absorption cross sections for *b*-cut Nd-doped niobate crystals.

### 2.3.2. Fluorescence spectra and decay times for Nd-doped crystals

The fluorescence spectra and fluorescence decay times were measured using an Edinburgh FLSP 920 spectrometer. Fig.4 (a) shows the room temperature photoluminescence spectra of Nd-doped niobate crystals in the wavelength range of 850 to 1450 nm, which was recorded at the same condition. The strongest emission peaks for them are all located at around 1066 nm, which corresponds to the  ${}^4\text{F}_{3/2}$  to  ${}^4\text{I}_{11/2}$  transition of  $\text{Nd}^{3+}$  ions. The other two emission bands

with central wavelength of 890 and 1330 nm are corresponding to the  ${}^4\text{F}_{3/2}$  to  ${}^4\text{I}_{9/2}$  and  ${}^4\text{I}_{13/2}$  transitions of  $\text{Nd}^{3+}$  ions, respectively. The fluorescence decay curves of  ${}^4\text{F}_{3/2} \rightarrow {}^4\text{I}_{11/2}$  transition are presented in Fig.4 (b). With single exponential decay, the fluorescence lifetime of  ${}^4\text{F}_{3/2} \rightarrow {}^4\text{I}_{11/2}$  transition for Nd-doped YNO, GNO, GYNO and GLNO are fitted to be 152, 162, 158 and 176  $\mu\text{s}$ , respectively. The stimulated emission cross section ( $\sigma_{em}$ ) can be calculated from the fluorescence spectrum using the Fuchtbauer-Ladenburg (F-L) formula[49]:

$$\sigma_{em}(\lambda) = \frac{\lambda^5 \cdot I(\lambda)}{8\pi n^2 c \tau_{exp} \int \lambda I(\lambda) d\lambda}$$

Where  $I(\lambda)$  is the fluorescence intensity at wavelength  $\lambda$ ,  $c$  is the speed of light,  $\tau$  is the radiative lifetime and  $n$  is the refractive index. Herein, the calculated stimulated emission cross sections for Nd-doped niobate crystals at 1.06  $\mu\text{m}$  are listed in the

Table 1. More importantly, the  $\sigma_{em}$  for Nd-doped mixed crystals GYNO and GLNO is smaller than that of Nd-doped YNO, which shall be caused by the disorder structure in the mixed crystals. The small  $\sigma_{em}$  and long fluorescence lifetime for mixed niobate crystals will result in a high energy storage capacity, which is beneficial for their applications in Q-switched laser[50].

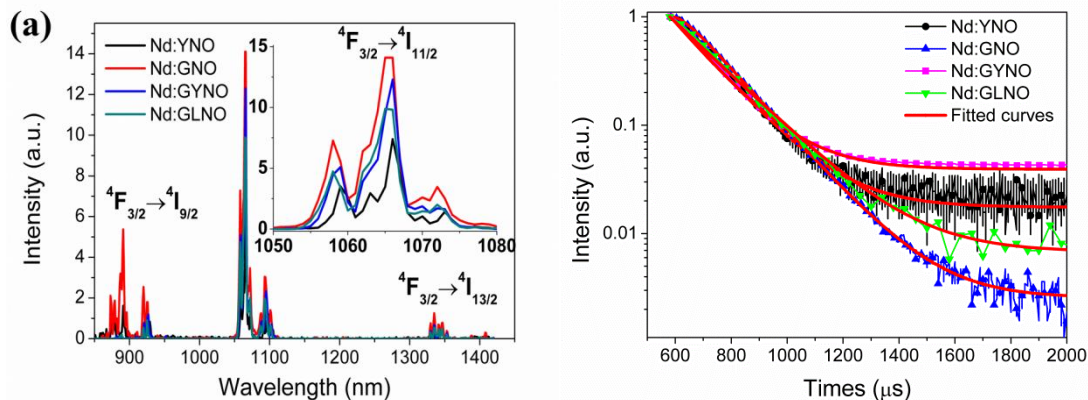


**Figure 4.** (a) emission spectra for Nd-doped niobate crystals excited at 808 nm; (b) Fluorescence decay curves for  ${}^4F_{3/2} \rightarrow {}^4I_{11/2}$  transition of  $\text{Nd}^{3+}$  in niobate crystals.

**Table 1.** The optical properties for Nd-doped niobate and tantalate crystals.

Crystals	$\sigma_{ab}$ ( $10^{-20}$ $\text{cm}^2$ at 808 nm)	$\sigma_{em}$ ( $10^{-20}$ $\text{cm}^2$ at 1066 nm)	$\tau$ ( $\mu\text{s}$ )
Nd:YNO	5.7	22	152
Nd:GNO	9.3	24	162
Nd:GYNO	11.7	20.5	158
Nd:GLNO	10.5	18	176
Nd:GdT <sub>2</sub> O <sub>7</sub>	5.1	39	178
(Nd:GTO)			
Nd:GdYTaO <sub>4</sub>	6.9	22	182
(Nd:GYTO)			

### 2.3.3. Absorption and fluorescence spectra for Yb-doped crystals

Yb ion has only two multiplets, ground state  ${}^2F_{7/2}$  and excited state  ${}^2F_{5/2}$ . This simple energy structure make many deleterious effects free from  $\text{Yb}^{3+}$  lasers, such as up-conversion, excited state absorption and cross-relaxation[51]. Moreover, owing to the maturing of high performance InGaAs diode lasers as pumping source in 900 to

1100 nm range[52],  $\text{Yb}^{3+}$  based solid state lasers have attracted more and more attentions[53-55]. In this work, we present the absorption and fluorescence spectra for Yb-doped niobate laser crystals, including 5 at% Yb-doped YNO and GNO, as showing in Fig.5. There are three obviously absorption peaks appeared in the wavelength range of 900 to 1000 nm for both of them. The peak positions for Yb:YNO are 933, 955 and 974 nm, whereas for Yb:GNO are 936, 955 and

975 nm, respectively. This slightly difference could be attributed to the small difference for the radius of  $Y^{3+}$  (0.9 Å) and  $Gd^{3+}$  (0.94 Å), and consequently to the small difference of the crystal field environment[56]. According to the absorption cross section calculation formula presented in the above, we calculated the absorption cross section for Yb-doped YNO and GNO as showing in the left ordinate of Fig.5. As can be seen, the  $\sigma_{ab}$  for Yb:YNO at 955 nm is almost twice than that of Yb:GNO, which means Yb:YNO could be more easily to generate laser. By contrast, CW laser has been achieved successfully in Yb:GNO (which will be discussed in the following part) rather than Yb:YNO crystal, which is because the Yb:YNO crystal quality obtained in the present stage is very poor. But it can foresee that if the crystal quality for Yb:YNO is improved, it will extremely

attractive for the laser applications. The emission spectrum for Yb-doped YNO and GNO is shown in the right ordinate of Fig.5. As we can see, both of them exhibit a very broad emission band from 970 to 1050 nm (contains three overlapped emission peaks located at around 1005, 1020 and 1030 nm, respectively) indicates that they are both potential candidates as novel near-infrared laser materials with LD pumping. Using the F-L formula mentioned above, the emission cross section for Yb-doped YNO are calculated to be 1.81, 1.11 and  $0.57 \times 10^{-20} \text{ cm}^2$  at 1005, 1021 and 1030 nm, respectively (for Yb:GNO are 0.45, 0.49 and  $0.47 \times 10^{-20} \text{ cm}^2$  at 1003, 1018 and 1030 nm, respectively). It is inspiring that the emission cross section for Yb:YNO is very close to that of Yb:YAG ( $2 \times 10^{-20} \text{ cm}^2$  at 1030 nm). As a result, Yb:YNO is very promising for generating high efficiency and high repetition rate laser.

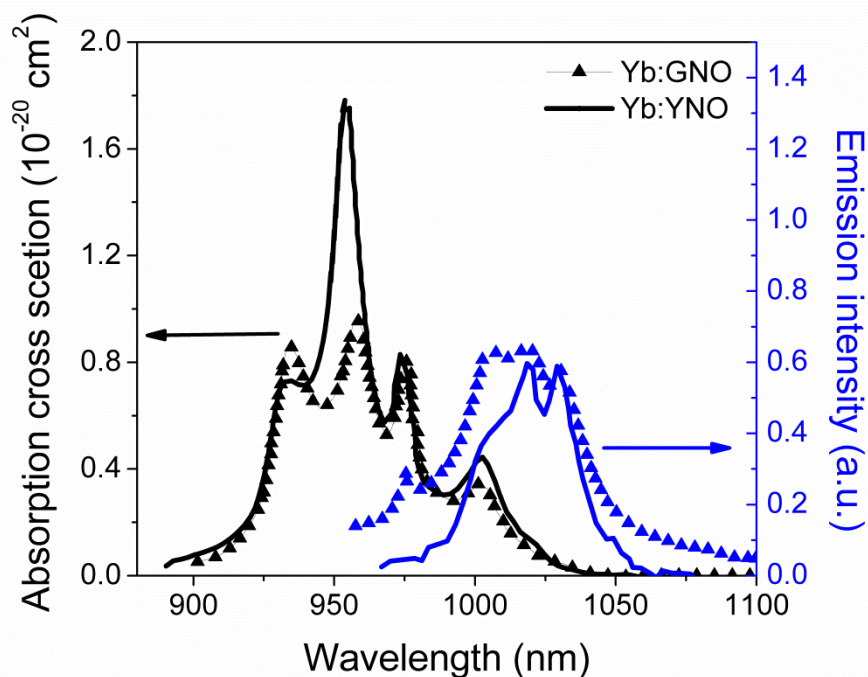


**Figure 5.** Absorption cross section for Yb-doped niobate crystals (left ordinate) and emission spectra for Yb-doped niobate crystals (right ordinate).

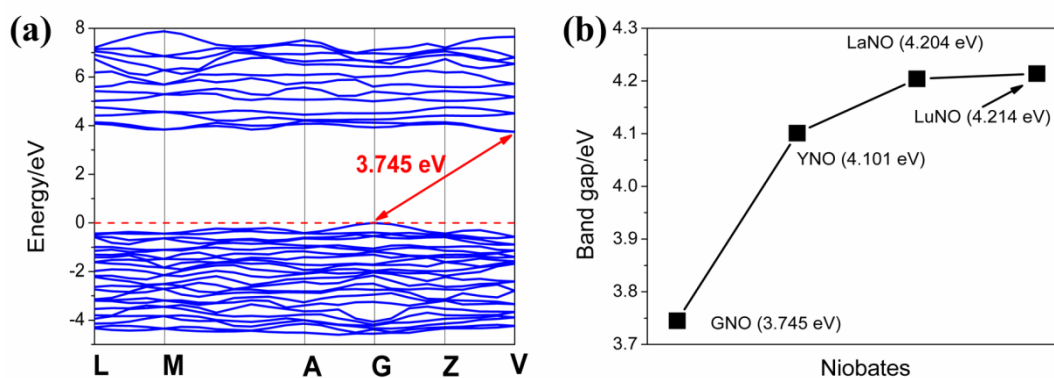
## 2.4. DFT calculations

### 2.4.1. Electronic structure

For luminescent materials, investigate their band structure is of great importance. Therefore, in this work, we calculated the electronic structure and optical properties for niobate materials using Cambridge Sequential Total Energy Package (CASTEP) within the framework of density functional theory (DFT)[57, 58]. The standard structure models with M-type used for calculation were adopted from the Findit software. The exchange-correlation (XC) energy of the electron-electron was treated under the generalized gradient approximation (GGA) according to the Perdew-Burke-Ernzerhof (PBE) function[59]. Considering the correlation effects are supposed to be of large importance in *d*- and *f*-electron systems, the quantum effects contributed by these strongly correlated *d*- and *f*- electrons was properly treated using the LDA+*U* approach[60, 61]. The valence electron configurations used in the computations were: Nb-4s<sup>2</sup>4p<sup>6</sup>4d<sup>4</sup>5s<sup>1</sup>, O-2s<sup>2</sup>2p<sup>4</sup>, Y-4d<sup>1</sup>5s<sup>2</sup>, Gd-4f<sup>7</sup>5s<sup>2</sup>5p<sup>6</sup>5d<sup>1</sup>6s<sup>2</sup>, La-5s<sup>2</sup>5p<sup>6</sup>5d<sup>1</sup>6s<sup>2</sup> and Lu-5d<sup>1</sup>5p<sup>6</sup>6s<sup>2</sup>4f<sup>14</sup>, respectively. Considering the same structure for niobates, in this work, we just take GNO as an example. The calculated band structure for GNO within -5 to 8 eV along with the high-symmetry points in

the first Brillouin zone is shown in Fig.6 (a). The maximum of the valance band (VB) and the minimum of the conduction band (CB) are located at *G* and *V* point, respectively, indicating that GNO belongs to the indirect band gap materials category. The calculated band gap for GNO is 3.745 eV, which is very close to that obtained in experiment (3.84 eV)[36]. In particular, we also calculated the band gap for YNO, LaNO and LuNO as showing in Fig.6 (b). It is obviously that there is a relatively large difference between the band gap of GNO and other niobates, which could be interpreted by the different luminescence mechanism between GNO and other niobates. In GNO host, the luminescence mechanism can be explained by the self-activated optical center related to the Gd<sup>3+</sup> and NbO<sub>4</sub><sup>3-</sup> group, whereas in other niobates (YNO, LaNO and LuNO) it just related to the NbO<sub>4</sub><sup>3-</sup> group[36].

Fig.6 (c) shows the calculated total density of states (DOS) and partial DOS for each constituent atom in GNO host. It can be seen that the bottom of the CB (4 to 8 eV, namely) is mainly occupied by O-2p state and partially hybridized with Nb-4d state, whereas the top of the VB (-5 to 0 eV, namely) is mainly dominated by Gd-4d state, indicating the covalent interaction between Gd-4d and O-2p in GNO matrix.



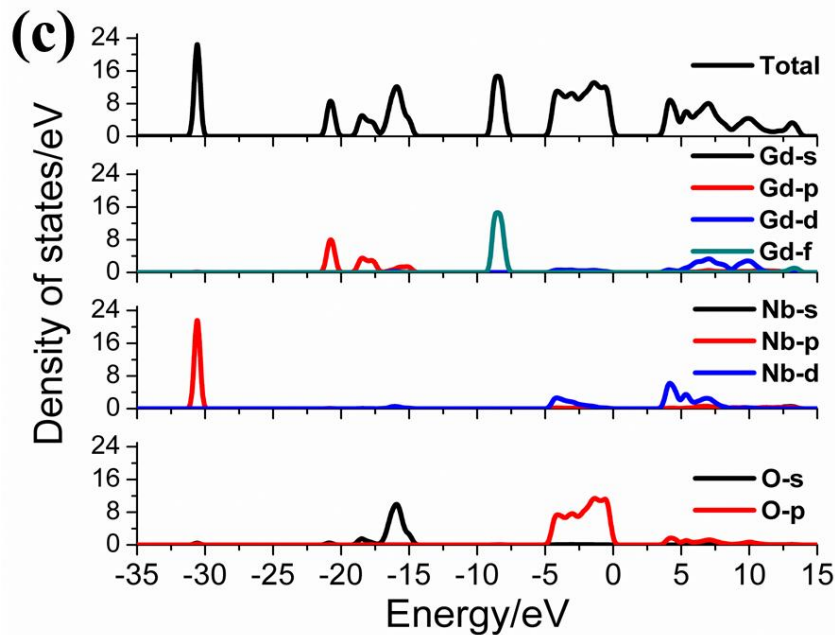


**Figure 6.** (a) The calculated band structure of  $\text{GdNbO}_4$ ; (b) The calculated band gap of  $\text{GdNbO}_4$ ,  $\text{YNbO}_4$ ,  $\text{LaNbO}_4$  and  $\text{LuNbO}_4$ ; (c) The calculated total density of states (DOS) and partial DOS for each constituent atom in GNO host.

#### 2.4.2. Refractive index and reflectivity

Refractive index and reflectivity are also especially important for the crystals used as optical elements. In this work, we present the refractive index and reflectivity for YNO and GNO with two methods: experimental and calculated. In experiment, their Sellmeier equations have been reported in our previous work[33, 41] and plotted in the Fig.7 (a). Compared with the calculated

results, it is inspiring that they are in good agreement, which confirms the reliability of our calculation results. As we know, reflectivity  $R$  can be calculated from the refractive index  $n$  using the following equation:

$$R = \left( \frac{n - 1}{n + 1} \right)^2$$

The calculated and experimental  $R$  is showing in Fig.7 (b). It is obviously that they are also in excellent agreement.

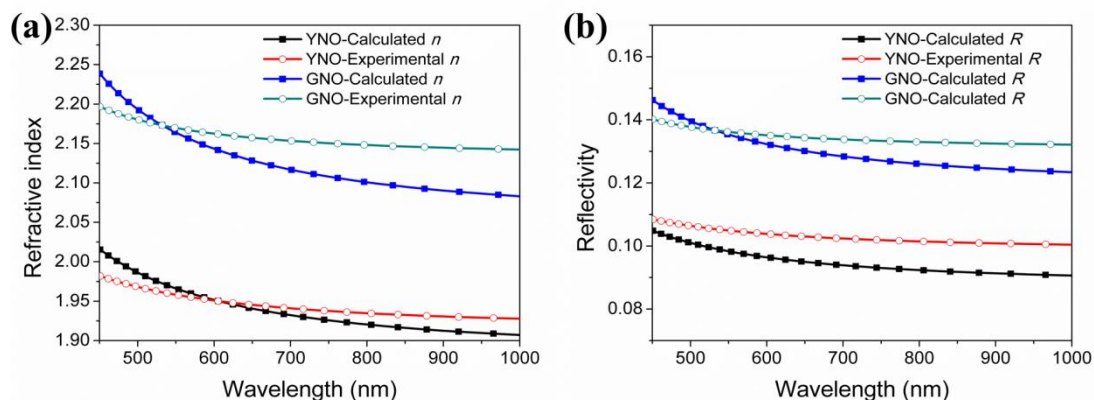


**Figure 7.** (a) The calculated and experimental refractive index for  $\text{GdNbO}_4$  and  $\text{YNbO}_4$ ; (b) The calculated and experimental reflectivity for  $\text{GdNbO}_4$  and  $\text{YNbO}_4$ .

### 3. Laser performances

#### 3.1. Continuous-wave laser performances

Diode pumped continuous wave laser experiments were performed using the following setup (Fig.8). The pumping beam was focused on the crystal through a focusing optics. M1 and M2 are input and output

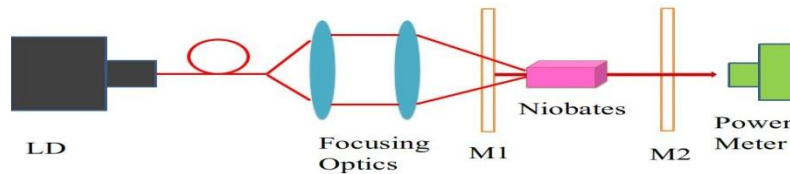


**Figure 8.** Schematic of the setup for the diode end-pumped continuous wave laser experiment.

##### 3.1.1. 1.06 $\mu\text{m}$ CW laser properties for Nd-doped niobate crystals

Considering the anisotropic property of the monoclinic system, we performed the laser experiment on niobate crystals in different crystalline orientations. The pumping source for Nd-doped niobate crystals is a fiber-coupled CW laser diode with a maximum output power of 30 W (central wavelength at around 808 nm). The transmittance for the output couple (M2) is 5.4% at 1.06  $\mu\text{m}$  for all the laser experiment. Fig.9 (a) and (b) shows the output powers under various incident pump powers using *b*- and *c*-orientated crystals, respectively. It can be seen that the pump threshold for Nd-doped niobate crystals are very close whatever in *b*- or *c*-orientation. The slope efficiency are

mirror, respectively. During the laser experiments, the crystals were mounted in a copper block and cooled by deionized water, in which the water temperature was maintained at 20  $^{\circ}\text{C}$ . The output laser power was measured using an OPHIR 30A-BB-18 power meter.

fitted to be 24%, 28% and 30% for *b*-orientated Nd:YNO, Nd:GNO and Nd:GYNO crystals, respectively. Besides, the slope efficiency are fitted to be 35%, 30% and 34% for *c*-orientated Nd:GNO, Nd:GYNO and Nd:GLNO crystal respectively. Compared with Nd-doped tantalate and vanadate crystals, niobate crystals exhibit lower CW laser slope efficiency, which could be explained by the following reasons: firstly, the niobate crystals used in the experiments were all uncoated; secondly, the concentration of the  $\text{Nd}^{3+}$  in niobate crystals were not optimized; thirdly, the plane-plane cavity used in the experiments were very crude. Therefore, the laser efficiency for niobate crystals are expected to be largely improved in the future works.

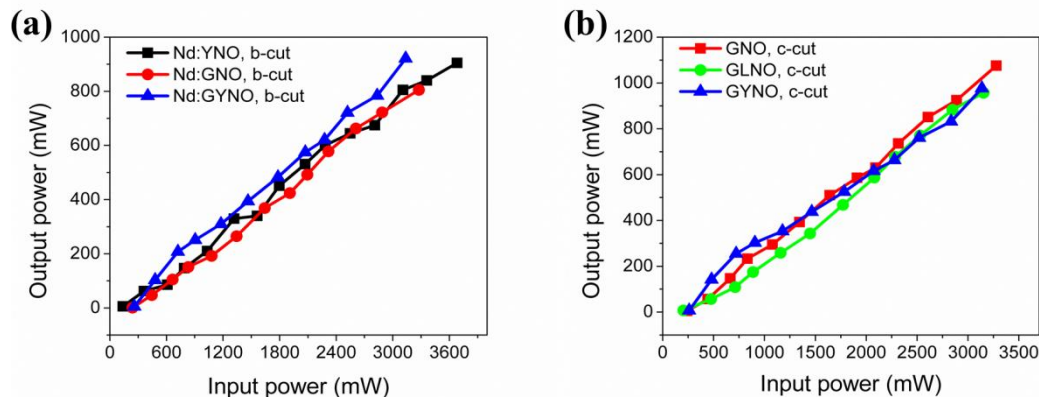


**Figure 9.** (a) 1.06  $\mu\text{m}$  continuous wave laser output power versus incident power for *b*-cut Nd-doped niobate crystals; (b) 1.06  $\mu\text{m}$  continuous wave laser output power versus incident power for *c*-cut Nd-doped niobate crystals.

### 3.1.2. 926 nm CW laser properties for Nd-doped GNO

926 nm laser operation in Nd:GNO crystal based on quasi-three-level  ${}^4F_{3/2} \rightarrow {}^4I_{9/2}$  transition was conducted in three crystalline orientations with different output coupling mirrors (M2 with transmittance of  $T=3.1\%$ ,  $6.0\%$  and  $11.6\%$ , respectively). The pumping source used in this experiment is a CW 120 W LD at 879 nm with a fiber core diameter of 400  $\mu\text{m}$ . Fig.10 (a) shows the CW laser experiment performed on the *a*-orientated Nd:GNO with different output coupling mirrors. As can be seen, the threshold is increased with the increasing of

the transmittance of the M2. Using a  $T=6.0\%$  plano-concave mirror, a highest laser output power of 393 mW at 926 nm was obtained, corresponding to a slope efficiency of 33.3% and an optical-to-optical efficiency of 26%. The slope efficiency with respect to absorbed pump power is estimated to be 47.7%. In addition, the CW laser performance at 926 nm using different orientated Nd:GNO crystals is shown in Fig.10 (b). As we can see, *a*-orientated Nd:GNO exhibits a better laser performance at 926 nm. All the results indicating that Nd-doped niobate crystal is also a promising material for laser generation around 900 nm.

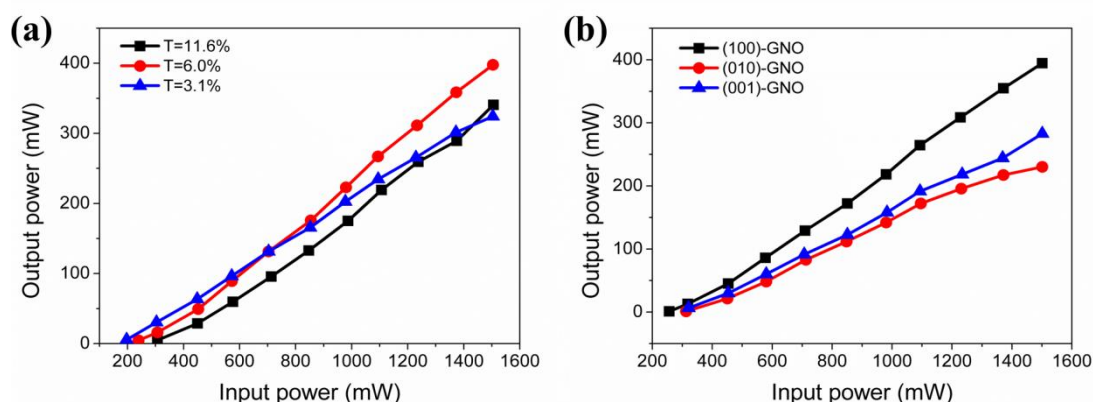


**Figure 10.** (a) 926 nm continuous wave laser output power versus incident power for Nd-doped niobate crystals with different transmission of the output coupler; (b) 926 nm continuous wave laser output power versus incident power for Nd-doped niobate crystals in three crystalline orientations.

### 3.1.3. CW laser properties for Yb-doped GNO

The preliminary CW laser experiment for Yb:GNO was also performed. The pump source is an InGaAs LD with a maximum output power of 25 W (central wavelength at 976 nm). The transmittance for the output couple (M2) is 3.54% at 1.03  $\mu\text{m}$ . A maxi-

imum laser output of 270 mW was achieved corresponding to a slope efficiency of 7.5%, as shown in Fig.11. Unfortunately, the threshold is as high as 7.5 W, which are mainly due to the crystal reabsorption and the poor quality of the as-grown crystal. In spite of this, the result indicates that niobate crystals are promising for Yb-doped lasers.

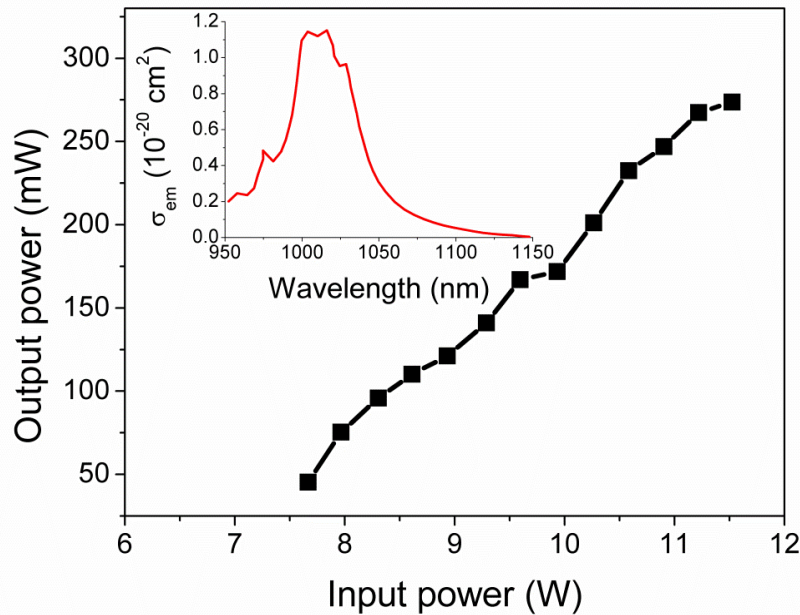


**Figure 11.** Continuous wave laser output power versus incident power for Yb:GdNbO<sub>4</sub> crystal. Inset: the emission cross section of Yb:GdNbO<sub>4</sub> crystal at room temperature.

**3.2. Passively Q-switched laser performances for Nd-doped niobate crystals**

In addition to the CW laser, the passively Q-switched lasers were also generated successfully using Nd-doped niobate crystals. The configuration of the passively Q-switched laser experiments under 808 nm fiber coupled LD end-pumping is shown in Fig.12. L1 and L2 are a set of collimating

and focusing lenses. M1 is a flat mirror with antireflection at 808 nm and high reflectivity at 1.06 μm. M2 is output coupler and its transmittance (*T*) has been optimized as 10%, 20% and 25% for Nd:GNO, Nd:GLNO and Nd:GYNO crystals. The transmittance for the used Cr<sup>4+</sup>:YAG saturable absorber is 90% and the laser cavity length is 40 mm for all the experiments.

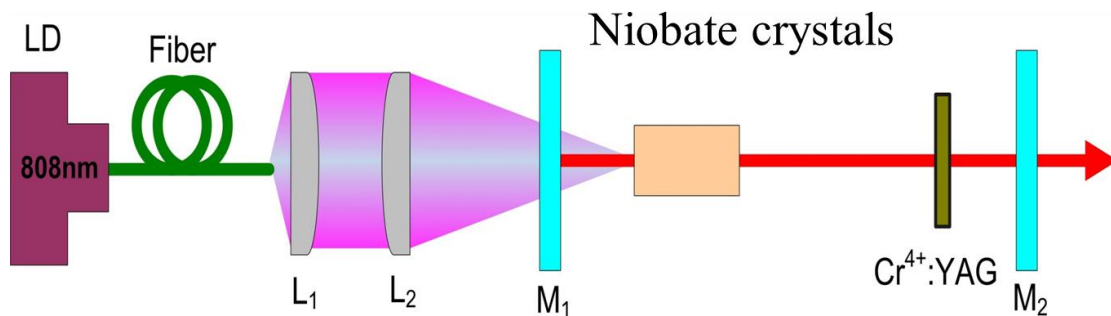


**Figure 12.** Schematic of the setup for the diode end-pumped passively Q-switched laser experiment.

Fig.13 (a) shows the average output power *P<sub>a</sub>* versus the incident pump power. As we can see, the thresholds for Nd-doped GNO, GYNO and GLNO crystals are 3.3, 6.5 and 4.5 W, respectively. Furthermore, the

maximum average output powers were achieved to be 0.41 W, 0.9 W and 0.89 W with Nd-doped GNO, GYNO and GLNO crystals respectively.

The pulse laser performances were measured by a high speed Si-detector and a digital oscillograph. The measured results of the pulse widths and the repetition rates were shown in Fig.13 (b) and (c). From Fig.13 (b), we can see that the pulse width ( $t_w$ ) decreases with the absorbed pump power for all of them. The obtained narrowest pulse widths for Nd-doped GNO, GYNO and GLNO crystals are 23, 12 and 32 ns, respectively. For repetition rate frequency (PRF), the maximum PRFs are achieved as 17.8, 39 and 24.5 kHz for Nd-doped GNO, GYNO and GLNO crystals respectively. Based on the obtained  $P_a$  and PRF, the pulse energy ( $E$ ) generated at  $P_{in}$  can be estimated by the formula:  $E=P_a/PRF$ . Fig.13 (d) shows the  $E$  versus  $P_{in}$  generated with different niobate crystals. The maximum pulse energy for Nd-doped GNO, GYNO and GLNO

crystals are 22.7, 24.2 and 36.4  $\mu$ J. The peak power ( $P_p$ ) can be calculated from the pulse energy and pulse width using the formula:  $P_p=E/t_w$ . The calculated peak power versus the incident pump power  $P_{in}$  for different niobate crystals is also shown in Fig.13 (d). The highest peak powers reached for Nd-doped GNO, GYNO and GLNO crystals are 0.97, 1.9, 1.1 kW, respectively.

Based on these results, we can conclude that Nd-doped niobate crystals also have great potentials in pulse laser application. It should be pointed out that we only performed the Q-switched lasers for Nd-doped niobate crystals using  $Cr^{4+}$ :YAG as saturable absorber, therefore, it could be foreseen that more fruitful Q-switched lasers will be obtained using other saturable absorber such as  $MoS_2$ , graphene oxide and so on in the future work.

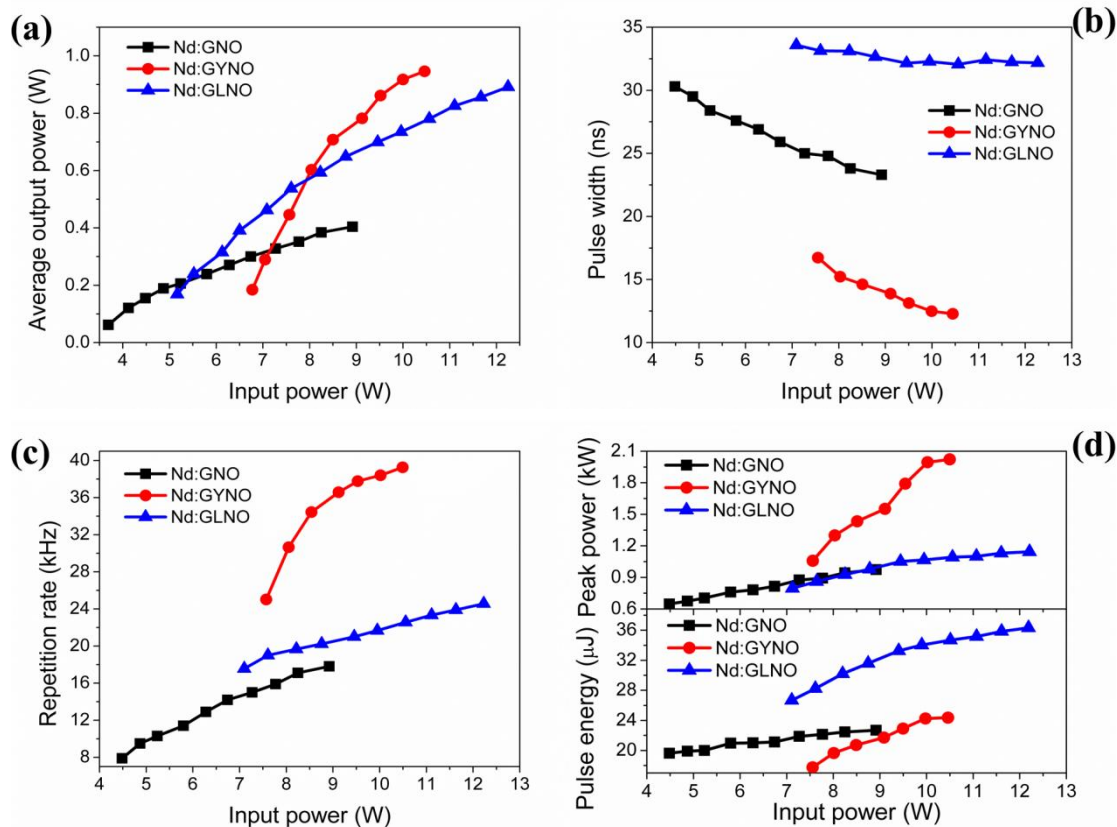


**Figure 13.** (a) Average output power versus absorbed pump power for Nd-doped niobate crystals; (b) Pulse width versus absorbed pump power for Nd-doped niobate crystals; (c) Repetition rate versus absorbed pump power for Nd-doped niobate crystals; (d) Pulse energy and pulse peak power versus absorbed pump power for Nd-doped niobate crystals.

#### 4. Conclusions

The niobate laser crystals involving Nd- and Yb-doped  $\text{YNbO}_4$ ,  $\text{GdNbO}_4$ ,  $\text{Gd}_{1-x}\text{Y}_x\text{NbO}_4$  and  $\text{Gd}_{1-x}\text{La}_x\text{NbO}_4$  were reviewed, including the growth, mechanical, luminescent and laser properties. Rare-earth doped niobate crystals exhibit some advantages over vanadate and tantalate crystals. For example, (a) niobate crystals have a lower melt point than that of tantalate crystals, suggesting that the larger-size crystal can be grown; (b) niobate crystals does not like vanadate crystals consist component volatility during the growth process, indicating that larger-size and higher-quality niobate crystals could be obtained. The Nd- and Yb-doped niobate crystals are all exhibit large full width at half maximum of absorption and emission spectra, which is advantageous for the low temperature dependence on temperature control of LD. In particular, the Yb-doped niobates, and mixed niobate crystals inherit the excellent properties of single crystals and possess large inhomogeneous spectral broadening, which are favorable for achieving pulsed lasers including Q-switching and mode locking. In conclusion, the niobate crystals have shown their great application prospective in lasers including continuous-wave, Q-switching and mode locking. It can be foreseen that with the development of solid-state lasers, the niobate crystals will play more and more important roles.

#### Acknowledgements

The National Natural Science Foundation of China (Grants No. 51502292, 51702322 and 61405206), National Key Research and Development Program of China (Grants No. 2016YFB0402101) and the China Scholarship Council (award Shoujun Ding study abroad at the Utah State University, Grants No.201706340135) supported this study.

#### Notes

The authors declare no competing financial interest.

#### REFERENCES

- [1] T.H. Maiman, Stimulated optical radiation in ruby, *Nature*, 187 (1960) 493.
- [2] Z. Kiss, R. Duncan, CROSS - PUMPED  $\text{Cr}^{3+}$ -  $\text{Nd}^{3+}$ : YAG LASER SYSTEM, *Appl. Phys. Lett.* , 5 (1964) 200-202.
- [3] T. Kajava, A.L. Gaeta, Q switching of a diode-pumped Nd: YAG laser with GaAs, *Opt. Lett.* , 21 (1996) 1244-1246.
- [4] D. Kuizenga, D. Phillion, T. Lund, A. Siegman, Simultaneous Q-switching and mode-locking in the cw Nd: YAG laser, *Opt Commun*, 9 (1973) 221-226.
- [5] J.A. Morris, C.R. Pollock, Passive Q switching of a diode-pumped Nd: YAG laser with a saturable absorber, *Opt. Lett.* , 15 (1990) 440-442.
- [6] P. Yankov,  $\text{Cr}^{4+}$ : YAG Q-switching of Nd: host laser oscillators, *J. Phys. D: Appl. Phys.* , 27 (1994) 1118.
- [7] S. Ding, F. Peng, Q. Zhang, J. Luo, W. Liu, D. Sun, R. Dou, J. Gao, G. Sun, M. Cheng, Crystal growth, spectral properties, and continuous wave laser operation of Nd:  $\text{GdNbO}_4$ , *J. Alloys Compd.* , 693 (2017) 339-343.
- [8] A. Ikesue, K. Kamata, K. Yoshida, Synthesis of  $\text{Nd}^{3+}$ ,  $\text{Cr}^{3+}$  - codoped YAG Ceramics for High - Efficiency Solid - State Lasers, *J. Am. Ceram. Soc.* , 78 (1995) 2545-2547.
- [9] K.Y. Yamamoto, D.A. Cremers, M.J. Ferris, L.E. Foster, Detection of metals in

the environment using a portable laser-induced breakdown spectroscopy instrument, *Appl. Spectrosc.* , 50 (1996) 222-233.

[10] D. Gu, W. Meiners, K. Wissenbach, R. Poprawe, Laser additive manufacturing of metallic components: materials, processes and mechanisms, *Int. Mater. Rev.* , 57 (2012) 133-164.

[11] S. Sivaprakasam, K. Shore, Signal masking for chaotic optical communication using external-cavity diode lasers, *Opt. Lett.* , 24 (1999) 1200-1202.

[12] C. Sibata, V. Colussi, N. Oleinick, T. Kinsella, Photodynamic therapy: a new concept in medical treatment, *Braz J Med Biol Res*, 33 (2000) 869-880.

[13] T. Ditmire, J. Zweiback, V. Yanovsky, T. Cowan, G. Hays, K. Wharton, Nuclear fusion from explosions of femtosecond laser-heated deuterium clusters, *Nature*, 398 (1999) 489.

[14] R.I. Kodama, H. Shiraga, K. Shigemori, Y. Toyama, S. Fujioka, H. Azechi, H. Fujita, H. Habara, T. Hall, Y. Izawa, Nuclear fusion: Fast heating scalable to laser fusion ignition, *Nature*, 418 (2002) 933.

[15] S. Zhao, H. Zhang, J. Wang, H. Kong, X. Cheng, J. Liu, J. Li, Y. Lin, X. Hu, X. Xu, Growth and characterization of the new laser crystal Nd: LuVO<sub>4</sub>, *Opt. Mater.* , 26 (2004) 319-325.

[16] D. Zhou, X. Xu, J. Meng, D. Li, J. Di, C. Xia, F. Wu, J. Xu, Spectroscopic analysis and lasing properties of Nd: Y<sub>2</sub> 5Gd<sub>0</sub>. 5Al<sub>5</sub>O<sub>12</sub> crystals, *Laser Phys. Lett.* , 8 (2011) 201.

[17] A. Zagumennyĭ, V. Ostroumov, I.A.

Shcherbakov, T. Jensen, J. Meyen, G. Huber, The Nd: GdVO<sub>4</sub> crystal: a new material for diode-pumped lasers, *Sov. J. Quantum Electron.* , 22 (1992) 1071.

[18] H. Yu, J. Liu, H. Zhang, A.A. Kaminskii, Z. Wang, J. Wang, Advances in vanadate laser crystals at a lasing wavelength of 1 micrometer, *Laser Photonics Rev.* , 8 (2014) 847-864.

[19] H. Yu, H. Zhang, J. Wang, Growth and Characterization of Vanadate Laser Crystals, *Acta Phys. Pol., A* 124 (2013) 301-304.

[20] R. Fields, M. Birnbaum, C. Fincher, Highly efficient Nd: YVO<sub>4</sub> diode - laser end - pumped laser, *Appl. Phys. Lett.* , 51 (1987) 1885-1886.

[21] M. Frede, R. Wilhelm, D. Kracht, 250 W end-pumped Nd: YAG laser with direct pumping into the upper laser level, *Opt. Lett.* , 31 (2006) 3618-3619.

[22] A. Kaminskii, High - temperature spectroscopic investigation of stimulated emission from lasers based on crystals activated with Nd<sup>3+</sup> ions, *physica status solidi (a)*, 1 (1970) 573-589.

[23] Y. Sato, T. Taira, The studies of thermal conductivity in GdVO<sub>4</sub>, YVO<sub>4</sub>, and Y<sub>3</sub>Al<sub>5</sub>O<sub>12</sub> measured by quasi-one-dimensional flash method, *Opt. Express* 14 (2006) 10528-10536.

[24] W. Koechner, Properties of solid-state laser materials, in: *Solid-State Laser Engineering*, Springer, 2006, pp. 38-101.

[25] Y. Zhang, G. Wang, Spectroscopic properties of Nd: Sr<sub>3</sub>Gd<sub>2</sub> (BO<sub>3</sub>)<sub>4</sub>, *physica status solidi (a)*, 209 (2012) 1128-1133.

[26] J. Hong, L. Zhang, J. Li, Z. Wang, J. He,

P. Zhang, Y. Wang, Y. Hang, Spectroscopic, thermal and cw dual-wavelength laser characteristics of Nd: LaF<sub>3</sub> single crystal, *Opt. Mater.* , 53 (2016) 10-13.

[27] A. Ballman, S.P.d.S. Porto, A. Yariv, Calcium niobate Ca (NbO<sub>3</sub>)<sub>2</sub>—a new laser host crystal, *J. Appl. Phys.* , 34 (1963) 3155-3156.

[28] D. Lu, Z. Pan, H. Yu, H. Zhang, J. Wang, Exploration of Yb<sup>3+</sup>: ScBO<sub>3</sub>-a novel laser crystal in the rare-earth ion doped orthoborate system, *Optical Materials Express*, 5 (2015) 1822-1833.

[29] M. Pujol, M. Bursukova, F. Güell, X. Mateos, R. Solé, J. Gavaldà, M. Aguiló, J. Massons, F. Díaz, P. Klopp, Growth, optical characterization, and laser operation of a stoichiometric crystal KYb (WO<sub>4</sub>)<sub>2</sub>, *Phys. Rev. B*, 65 (2002) 165121.

[30] F. Peng, H. Yang, Q. Zhang, J. Luo, W. Liu, D. Sun, R. Dou, G. Sun, Spectroscopic properties and laser performance at 1,066 nm of a new laser crystal Nd: GdTaO<sub>4</sub>, *Appl. Phys. B* 118 (2015) 549-554.

[31] G. Blasse, Luminescence processes in niobates with fergusonite structure, *J. Lumin.* , 14 (1976) 231-233.

[32] E. Karsu, E. Popovici, A. Ege, M. Morar, E. Indrea, T. Karali, N. Can, Luminescence study of some yttrium tantalate-based phosphors, *J. Lumin.* , 131 (2011) 1052-1057.

[33] S. Ding, F. Peng, Q. Zhang, J. Luo, W. Liu, D. Sun, R. Dou, G. Sun, Structure, spectroscopic properties and laser performance of Nd: YNbO<sub>4</sub> at 1066 nm, *Opt. Mater.* , 62 (2016) 7-11.

[34] C. Balamurugan, D.-W. Lee, A.

Subramania, Preparation and LPG-gas sensing characteristics of p-type semiconducting LaNbO<sub>4</sub> ceramic material, *Appl. Surf. Sci.* , 283 (2013) 58-64.

[35] R. Haugrud, B. Ballesteros, M. Lira-Cantú, T. Norby, Ionic and electronic conductivity of 5% Ca-doped GdNbO<sub>4</sub>, *J. Electrochem. Soc.* , 153 (2006) J87-J90.

[36] S. Ding, H. Zhang, Q. Zhang, Y. Chen, R. Dou, F. Peng, W. Liu, D. Sun, Experimental and first principle study of the structure, electronic, optical and luminescence properties of M-type GdNbO<sub>4</sub> phosphor, *J. Solid State Chem.* , (2018).

[37] J. Pellicer-Porres, A. Garg, D. Vázquez-Socorro, D. Martínez-García, C. Popescu, D. Errandonea, Stability of the fergusonite phase in GdNbO<sub>4</sub> by high pressure XRD and Raman experiments, *J. Solid State Chem.* , 251 (2017) 14-18.

[38] A. Dwivedi, A. Singh, S. Rai, Down-shifting and upconversion photoluminescence in Ho<sup>3+</sup>/Yb<sup>3+</sup> codoped GdNbO<sub>4</sub>: effect of the Bi<sup>3+</sup> ion and the magnetic field, *Dalton Trans.* , 43 (2014) 15906-15914.

[39] R. Dou, Q. Zhang, J. Luo, J. Chen, H. Yang, W. Liu, G. Sun, D. Sun, Growth, structure, and spectroscopic properties of 5 at.% Yb: GdNbO<sub>4</sub> laser crystal, *Opt. Mater.* , 42 (2015) 56-61.

[40] S. Ding, Q. Zhang, J. Gao, W. Liu, J. Luo, D. Sun, G. Sun, X. Wang, Growth, structure, spectral properties and crystal-field analysis of monoclinic Nd: YNbO<sub>4</sub> single crystal, *Physica B* 503 (2016) 106-110.

[41] S. Ding, Q. Zhang, J. Luo, W. Liu, X. Wang, G. Sun, X. Li, D. Sun, Thermal, de-

fects, mechanical and spectral properties of Nd-doped GdNbO<sub>4</sub> laser crystal, *Appl. Phys. A* 123 (2017) 335.

[42] R. Yan, X. Li, W. Yao, Y. Shen, Z. Zhou, F. Peng, Q. Zhang, R. Dou, J. Gao, 926 nm laser operation in Nd: GdNbO<sub>4</sub> crystal based on 4F<sub>3/2</sub>→4I<sub>9/2</sub> transition, *Opt. Laser Technol.*, 101 (2018) 515-519.

[43] S. Ding, Q. Zhang, W. Liu, J. Luo, F. Peng, X. Wang, G. Sun, D. Sun, Crystal growth and characterization of a mixed laser crystal: Nd-doped Gd 0.89 La 0.1 NbO<sub>4</sub>, *RSC Advances*, 7 (2017) 35666-35671.

[44] S. Ding, Q. Zhang, F. Peng, W. Liu, J. Luo, R. Dou, G. Sun, X. Wang, D. Sun, Crystal growth, spectral properties and continuous wave laser operation of new mixed Nd: GdYNbO<sub>4</sub> laser crystal, *J. Alloys Compd.*, 698 (2017) 159-163.

[45] S. Ding, Q. Zhang, J. Luo, W. Liu, W. Lu, J. Xu, G. Sun, D. Sun, Crystal growth, structure, defects, mechanical and spectral properties of Nd<sub>0.01</sub>:Gd<sub>0.89</sub>La<sub>0.1</sub>NbO<sub>4</sub> mixed crystal, *Appl. Phys. A* 123 (2017) 636.

[46] S. Ding, Q. Zhang, J. Luo, W. Liu, D. Sun, X. Wang, G. Sun, J. Gao, Basic Properties of Nd - Doped GYSGG Laser Crystal, *Cryst. Res. Technol.*, 52 (2017).

[47] Y. Ma, H. Sun, Z. Peng, S. Ding, F. Peng, X. Yu, Q. Zhang, Diode-pumped continuous-wave and passively Q-switched Nd: GdLaNbO<sub>4</sub> laser, *Optical Materials Express*, 8 (2018) 983-991.

[48] H. Xu, H. Yu, Z. Wang, S. Han, Y. Wang, Z. Pan, Y. Zhang, S. Sun, J. Wang, H. Zhang, Thermal and laser characteristics of Nd doped La 0.11 Y 0.89 VO<sub>4</sub> crystal, *Opt. Express* 20 (2012) 16524-16531.

[49] W. Krupke, M. Shinn, J. Marion, J. Caird, S. Stokowski, Spectroscopic, optical, and thermomechanical properties of neodymium-and chromium-doped gadolinium scandium gallium garnet, *JOSA B*, 3 (1986) 102-114.

[50] F. Peng, H. Yang, Q. Zhang, J. Luo, D. Sun, W. Liu, G. Sun, R. Dou, X. Wang, X. Xing, Growth, thermal properties, and LD-pumped 1066 nm laser performance of Nd<sup>3+</sup> doped Gd/YTaO<sub>4</sub> mixed single crystal, *Optical Materials Express*, 5 (2015) 2536-2544.

[51] F. Brunner, T. Südmeyer, E. Innerhofer, F. Morier-Genoud, R. Paschotta, V. Kisel, V. Shcherbitsky, N. Kuleshov, J. Gao, K. Contag, 240-fs pulses with 22-W average power from a mode-locked thin-disk Yb: KY (WO<sub>4</sub>)<sub>2</sub> laser, *Opt. Lett.*, 27 (2002) 1162-1164.

[52] S. Chen, W. Li, J. Wu, Q. Jiang, M. Tang, S. Shutts, S.N. Elliott, A. Sobiesierski, A.J. Seeds, I. Ross, Electrically pumped continuous-wave III–V quantum dot lasers on silicon, *Nat. Photonics* 10 (2016) 307.

[53] A. Demidovich, A. Kuzmin, G. Ryabtsev, M. Danailov, W. Strek, A. Titov, Influence of Yb concentration on Yb: KYW laser properties, *J. Alloys Compd.*, 300 (2000) 238-241.

[54] C. Tu, Y. Wang, Z. You, J. Li, Z. Zhu, B. Wu, Growth and spectroscopic characteristics of Ca<sub>3</sub>Gd<sub>2</sub>(BO<sub>3</sub>)<sub>4</sub>: Yb<sup>3+</sup> laser crystal, *J. Cryst. Growth* 265 (2004) 154-158.

[55] A. Brenier, G. Boulon, Overview of the best Yb<sup>3+</sup>-doped laser crystals, *J. Alloys Compd.*, 323 (2001) 210-213.

[56] R. Dou, Q. Zhang, J. Gao, Y. Chen, S. Ding, F. Peng, W. Liu, D. Sun, Rare-Earth

Tantalates and Niobates Single Crystals: Promising Scintillators and Laser Materials, *Crystals*, 8 (2018) 55.

[57] S. Baroni, S. De Gironcoli, A. Dal Corso, P. Giannozzi, Phonons and related crystal properties from density-functional perturbation theory, *Rev. Mod. Phys.* , 73 (2001) 515.

[58] M. Segall, P.J. Lindan, M.a. Probert, C. Pickard, P.J. Hasnip, S. Clark, M. Payne, First-principles simulation: ideas, illustrations and the CASTEP code, *J. Phys.: Condens. Matter* 14 (2002) 2717.

[59] J.P. Perdew, K. Burke, M. Ernzerhof, Generalized gradient approximation made simple, *Phys. Rev. Lett.* , 77 (1996) 3865.

[60] S. Ding, A. Kinross, X. Wang, H. Yang, Q. Zhang, W. Liu, D. Sun, Experiment and density functional theory analyses of GdTaO<sub>4</sub> single crystal, *Solid State Commun.* , 273 (2018) 5-10.

[61] T.L. Lim, M. Nazarov, T.L. Yoon, L.C. Low, M.A. Fauzi, X-ray diffraction experiments, luminescence measurements and first-principles GGA+ U calculations on YTaO<sub>4</sub>, *Comput. Mater. Sci.* , 77 (2013) 13-18.